



Pre- and post-simulations of shake-table tests on a stone masonry building aggregate using finite-discrete elements

O. AlShawa¹ · D. Liberatore¹ · L. Sorrentino¹

Received: 30 April 2022 / Accepted: 18 October 2022
© The Author(s) 2022

Abstract

This work presents the simulations of the non-linear dynamic response of a three-dimensional finite-discrete element model. The model simulates a half-scale masonry building aggregate tested on a shake table by other Authors. The aggregate is made of two un-connected building units having different heights and slightly different wall thicknesses. The floors are made of timber beams and boards. The modelling approach accounts jointly for in-plane and out-of-plane responses, which can be expected given the high flexibility of the floors, and for the separation between the two building units. The simulations are related both to the blind predictions, according to a scheduled testing sequence, and to the post-dictions according to the actual testing sequence and some model calibrations. The prediction model overestimates displacements, underestimates base shear and fairly predicts the damage pattern of comparable experimental runs. The use of the recorded shake table motion improves the accuracy of the post-diction simulations, while still delivering beam unseating. A higher Young's modulus of the blocks improves markedly the predictions. The strengthening intervention with steel angles connecting floors to walls is only approximately modelled and does not improve the outcomes of the simulations. In summary, the adopted modelling approach is capable of accounting for the pounding between the two building units, predicting the most significant damage as well as estimating approximate average of peak values of base shear and displacements, while individual time histories are less accurately estimated.

Keywords Historical masonry · Masonry building aggregate · Incremental dynamic analysis · Shake-table test · FEM-DEM · Earthquake response · Seismic behaviour

✉ L. Sorrentino
luigi.sorrentino@uniroma1.it

O. AlShawa
omar.alshawa@uniroma1.it

D. Liberatore
domenico.liberatore@uniroma1.it

¹ Department of Structural and Geotechnical Engineering, Sapienza – University of Rome, Via Antonio Gramsci 53, 00197 Roma, Italy

1 Introduction

Masonry building aggregates, also called blocks, clusters, compounds, conglomerations or precincts, represent one of the most common construction types in historical centres in regions with high seismic activity, and they are usually made of ordinary buildings (Carocci 2012), but may also comprise schools (Di Ludovico et al. 2017), heritage buildings (Sorrentino et al. 2014), churches (Marotta et al. 2015). Most of these buildings are not designed to withstand earthquake actions and frequently present a poor performance (Mazzoni et al. 2018). Aggregates are usually formed by assemblage and transformations of masonry buildings originally built independently. Therefore, building aggregates are the combination of different construction methods implemented at different times and with different materials (da Porto et al. 2013). The global behaviour of these structures depends on several factors: the geometry of the structure and its plan configuration, the connections between walls and between walls and floors, the stiffness of floors, and the interactions between adjacent buildings (Tomažević et al. 1991). The seismic assessment of building aggregates is not an easy task, and specific modelling guidelines are missing.

With the aim to investigate the response of building aggregates under seismic actions, a laboratory campaign was designed at the Seismology and Earthquake Engineering Research Infrastructure Alliance for Europe (SERA), and specifically within the Seismic Testing of Adjacent Interacting Masonry Structures (AIMS) program. The tests were performed at the Civil Engineering National Laboratory (LNEC) in Lisbon, Portugal, and a blind prediction competition was organised (Tomić et al. 2022a). The modelling strategy adopted by the authors for their blind predictions, as well as their post-dictions with the actual shake table motion, along with alternative modelling solutions are presented in the following.

Whereas ample literature exists about the numerical modelling of the earthquake response of unreinforced masonry buildings (e.g., Roca et al. 2010; D'Altri et al. 2020, and references therein) the numerical modelling of building aggregates has so far received limited attention. The most simplified approach relies on vulnerability index formulations, with partial scores and their weight given according to expert judgment (Valluzzi et al. 2005; Formisano et al. 2015; Maio et al. 2015; Cocco et al. 2019). An alternative approach relies on fragility functions associated to types to be found in aggregates (Ingham et al. 2018). Limit analysis was proposed for a predefined set of mechanisms (Valluzzi et al. 2005; Ingham et al. 2018) or selecting the most vulnerable ones by means of a finer discretisation resorting to non-uniform rational b-spline surfaces (Grillanda et al. 2020). Whenever good connections can be assumed, the use of the equivalent frame method was used in several instances for nonlinear static analyses (Pujades et al. 2012; Maio et al. 2015; Cocco et al. 2019; Grillanda et al. 2020).

Non-linear dynamic analyses were performed in very few cases on building aggregates. Senaldi et al. (2010), used an equivalent frame model to compare the dynamic response of idealized building units being either isolated or belonging to an aggregate. In the second case all building units were considered fully connected. The same assumption was made by Senaldi et al. (2019), when replicating the experimental behaviour of a building aggregate, using an enriched equivalent frame approach accounting for the out-of-plane stiffness of transverse walls and gables. This approach was further developed by Vanin et al. (2020), who replicated shaking table experimental tests accounting also for the out-of-plane flexural response of macro-elements and for finite-strength floor-to-wall and wall-to-wall connections. This strategy has the potential to account for pounding phenomena but, given the

lack of substantial damage at the interface between the two building units of the experimental aggregate, the corresponding adjacent piers were modelled as a single element. Stavroulaki (2019) modelled real and idealized building aggregates using the finite element method. The aim of the research was to evaluate which boundary conditions should be assumed when an individual building unit, belonging to a building aggregate, is modelled and to compare the effect of interventions on individual floors of the aggregate. When the whole building aggregate was modelled, a full connection between building units was assumed. The finite element method was used to model existing case studies by Grillanda et al. (2020) and by Malcata et al. (2020), who again modelled adjacent building units as fully connected.

Hence, in none of the previous cases the presence of joints active only in compression was considered as will be done in the following.

2 Test specimen summary

2.1 Geometry, details and material properties

A natural-stone masonry, 1:2 scale model of a building aggregate was built and tested within the SERA-AIMS program. The aggregate was made by two adjacent building units with different storey and total heights (Fig. 1a). The unreinforced masonry was made of undressed natural stone units and of a special mortar to reduce its strength and account for the scale of the model (Senaldi et al. 2020) (Fig. 1b). The physical model had two cells of side approximately equal to 2.5 m (Fig. 2). Unit 1 had one storey, was 2.20 m tall and its walls were 0.30 m thick; Unit 2 had two storeys, was 3.15 m tall and its walls were 0.35 m thick at ground level, and 0.25 m thick at the upper level. Unit 2 was built before Unit 1 and the two units were not interlocked, with a thin mortar layer separating them. The floors were made of very flexible, one-way timber beams and boards, with different orientations for the two building units. The lintels were made of timber as well. The geometry of the specimen was symmetric in plan with respect to the longitudinal axis, parallel to Y .

The full description of the test specimen and the results of incremental dynamic shake-table tests, complemented by material and component characterisation tests, are presented in Tomić et al. (2022b). In Table 1 the main experimental material properties, obtained after tests on wallettes, are summarised.



Fig. 1 Physical model: **a** General view and **b** Masonry geometric bond pattern (Tomić et al. 2019)

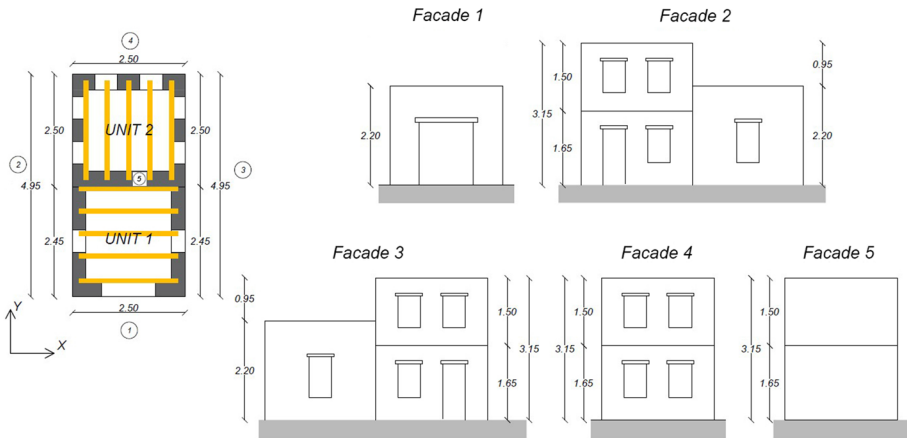


Fig. 2 Case study of the stone masonry aggregate experimental campaign (adapted after Tomić et al. 2019). Floor plan with beam orientation and facade layout of the two building units

Table 1 Experimental mean material properties (adapted after Tomić et al. 2022b)

Property	Mean
Density; ρ [Mg/m^3]	1.980
Compressive strength; f [MPa]	1.300
Tensile strength; f_t [MPa]	0.170
Cohesion; f_{v0} [MPa]	0.233
Poisson's modulus; ν [-]	0.140
Young's modulus in compression; E [GPa]	3.462
Shear modulus ^a ; G [GPa]	1.524
Shear modulus ^b ; G [GPa]	1.898

^afrom vertical compression test

^bfrom diagonal compression test

2.2 Earthquake record and testing sequences

The specimen was tested under one or two horizontal components recorded at the Albatros station during the Montenegro 1979 earthquake. The E-W and the N-S components have natural peak ground acceleration (PGA) 0.21 g and 0.18 g, respectively. To account for the model scale, the time of the records was scaled by a $1/\sqrt{2}$ factor. The incremental shake-table tests were scheduled to be performed applying to the ground motion amplitude the following scale factors: 25, 50, 75 and 100% of the table capacities that are 0.875 g in the Y direction and 0.625 g in the X direction (Tomić et al. 2022b). At each intensity level, three tests were planned (always in the same order): Y-direction (longitudinal); X-direction (transversal); test simultaneously in both the X- and the Y-direction (Table 2).

To calibrate the shake table, and based on observed damage, the actual testing sequence was markedly different from the planned one and is reported in Table 3. After the 7th run, it was decided to strengthen the physical model by fixing the floors to their walls employing $100 \times 100 \text{ mm}^2$ steel angles, 80 mm long when connected to the beam end or 160 mm

Table 2 Scheduled blind prediction testing sequence (adapted after Tomić et al. 2022a)

Run notation	Direction	Nominal <i>PGA</i> [g]
B1.1	<i>Y</i>	0.219
B1.2	<i>X</i>	0.156
B1.3	<i>Y & X</i>	0.219 (<i>Y</i>), 0.156 (<i>X</i>)
B2.1	<i>Y</i>	0.438
B2.2	<i>X</i>	0.313
B2.3	<i>Y & X</i>	0.438 (<i>Y</i>), 0.313 (<i>X</i>)
B3.1	<i>Y</i>	0.656
B3.2	<i>X</i>	0.469
B3.3	<i>Y & X</i>	0.656 (<i>Y</i>), 0.469 (<i>X</i>)
B4.1	<i>Y</i>	0.875
B4.2	<i>X</i>	0.625
B4.3	<i>Y & X</i>	0.875 (<i>Y</i>), 0.625 (<i>X</i>)

Table 3 Experimental sequence of the SERA-AIMS shake-table tests (adapted after Tomić et al. 2022b). S suffix related to strengthened specimen

Run notation	Direction	Recorded <i>PGA</i> [g]
E0.1	<i>Y</i>	0.113
E0.2	<i>X</i>	0.075
E0.3	<i>Y & X</i>	0.114 (<i>Y</i>), 0.072 (<i>X</i>)
E1.1	<i>Y</i>	0.170
E1.2	<i>X</i>	0.178
E1.3	<i>Y & X</i>	0.208 (<i>Y</i>), 0.174 (<i>X</i>)
E2.1	<i>Y</i>	0.593
E2.1S	<i>Y</i>	0.615
E1.2S	<i>X</i>	0.258
E2.2S	<i>X</i>	0.425

long when connected along the beam length. The two acceleration record sequences are compared in Fig. 3 for the *Y* and *X* directions. Based on relevant response spectra accelerations, Tomić et al. (2022a) selected blind prediction quantities to be compared to specific experimental quantities (Table 4). These comparisons will be extended in the following to post-dictions corresponding to experimental runs.

3 Numerical modelling

3.1 Modelling hypotheses

In previous studies the authors investigated problems similar to that considered here, such as full wall enclosures (Abrams et al. 2017), wall assemblies without roof (AlShawa et al. 2017) under horizontal and vertical ground motion (Liberatore et al. 2019), multiple wythes wall sections (de Felice et al. 2022), but never before building aggregates. Hence, a three-dimensional finite element method - discrete element method (FEM-DEM) non-linear dynamic model is implemented within LS-DYNA (Hallquist 2006) to simulate the

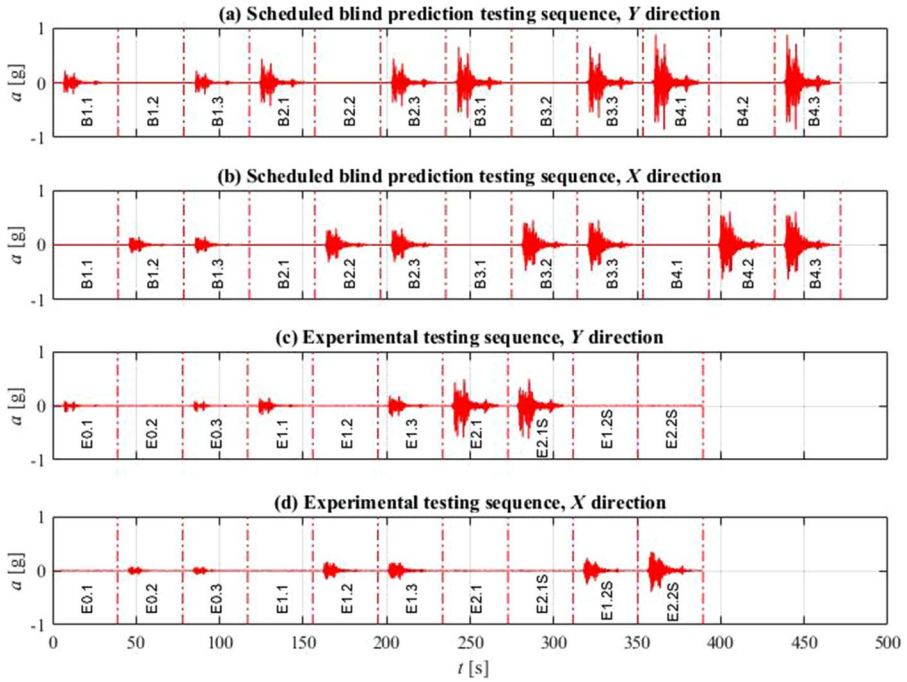


Fig. 3 Scheduled blind prediction sequence of acceleration records: **a** Y direction, **b** X direction. Experimental sequence of the SERA AIMS shake-table tests: **c** Y direction, **d** X direction

Table 4 List of quantities related to blind scheduled runs comparable with experimental runs to account for differences between nominal and effective shake table accelerations (Tomic et al. 2022a)

Blind run	Experimental run	Compared quantities
B1.3	E1.3	Rd2, Rd3, Rd4, Rd5, Rd6; Id1, Id2, Id3, Id4; BSX, BSY
B3.1	E2.1	Rd2, Id3, BSY
B3.2	E2.2S	Rd3, Id4, BSX

Rd=roof displacement relative to table, Id=interface opening, i.e. Unit 2 displacement relative to Unit 1 (Fig. 4), BSi=Base Shear in the i -th direction

prototype response to earthquake records. The modelling approach accounts jointly for in-plane and out-of-plane responses, which can be expected given the high flexibility of the floors.

Masonry is idealized with three-dimensional solid blocks each other separated by cohesive-frictional contact interfaces. Each block corresponds to several physical masonry units, their mortar joints in-between and half mortar joint on the boundary, given that the interface has zero thickness. Blocks are meshed into several 8-node solid FEs that adopt one integration point (constant stress formulation) and viscous hourglass control based on Flanagan and Belytschko (1981). Hereinafter a linear-elastic behaviour will be assumed

for these FEs, hence crushing is not accounted for. As in DEM, cracking, separation and formation of new contacts can be taken into account thanks to the interfaces. However, contrary to DEM, at the interface there are no additional springs, while the interface force depends on an automatic spring, whose stiffness is determined by geometry and material properties of the two bodies in contact, according to a penalty approach (AlShawa et al. 2017).

The adopted strategy for the contact allows the connections to transmit both compressive and tensile forces, with optional failure criteria for the latter. The adopted spring failure criterion is based on tensile normal stress, with failure occurring when the following inequality is satisfied:

$$\sigma_n \geq NFLS \quad (1)$$

where σ_n is the normal stress on the contact surface.

$NFLS$ is the normal (tensile) failure limit stress.

Once $NFLS$ is exceeded no tensile stress can be transmitted across the interface. The shear response is governed by a Mohr-Coulomb model, defined by a cohesion named shear failure limit stress ($SFLS$) and by static and dynamic friction coefficients (FS , FD).

The equations of motion are solved using an explicit strategy, capable to investigate crack propagation and dynamic response.

3.2 Blind prediction model configuration

The model implemented for the blind prediction is shown in Fig. 5. Despite the actual masonry having a random-irregular geometric bond pattern (Fig. 1), the numerical model has a periodic block distribution with parallelepiped blocks. This strong assumption is related to the explicit algorithm implemented to solve the equations of motion, with the smallest FE governing the integration time step. However, it is worth to emphasise that the actual bond pattern, across the masonry volume, is impossible to know outside a laboratory and numerical simulations of bond patterns prone to disintegration can be rather sensitive to geometric details, as discussed in de Felice et al. (2022). Therefore, a simplified geometry was assumed that, although not matching the actual bond pattern of the masonry, accounts for multiple failure planes. Conceptually, this approach is similar to the limit-analysis finer discretization (without a strict mimic of the actual construction) performed using non-uniform rational b-spline surfaces (Grillanda et al. 2020) instead of predefining a response mechanism (Valluzzi et al. 2005). In the sensitivity analyses performed for the post-dictions an alternative geometric bond pattern will be considered.

The size of the blocks was chosen so that all walls have two blocks across the thickness, with the only exception of single-wythe spandrels, but a finer discretisation was avoided to limit the already challenging computational burden. Hence, masonry blocks have the following size: maximum 450 mm, minimum 100 mm, with a typical block being $300 \times 150 \times 125 \text{ mm}^3$ ($w \times d \times h$). The total number of blocks is 1545 and the total number of FEs is 4687. No bond-stones (through-thickness headers) are present, not even close to the openings. The adopted geometric bond pattern may overestimate actual corner interlocking stiffness and capacity if an interlocking unit is present every other course; therefore, it is implemented only every five or six courses.

Because the floors are very flexible and are not anchored to the walls, no diaphragm kinematic restraint is assumed. As already discussed about masonry geometric bond pattern,

to avoid small-size FEs that would increase computation time, the rather thin boards are not modelled, and tributary masses are added to the beams. Additionally, the height of the lintels is slightly increased to match the height of the adjacent masonry course.

The values of the stress limits of the contact interfaces between the blocks are reported in Table 5 and, as a first approximation, are derived from those in Table 1. These values were used in the simulation of a diagonal-compression test of a wallette having the same geometric bond pattern of the building aggregate model. Failure was attained for a diagonal force very close to the average one reported by Tomić et al. (2022b). The comparison of the experimental and numerical results, related to the building aggregate, presented in the following will show that experimental model strength is reasonably estimated, corroborating the choice of stress limits.

The collar joint between the two wythes has the same mechanical characteristics of the interface between two blocks, whereas the interface between the two building units has a conventional tensile strength of 0.1 kPa, much lower than that assumed between two blocks, to capture their separation and possible pounding. Moreover, for the blind prediction, the interface between timber beams and masonry blocks has the same characteristics of that between the two building units (Table 5). In the sensitivity analyses performed for the post-dictions alternative properties will be considered. On the contrary, the interface between timber lintels and masonry blocks has the same characteristics of that between two masonry blocks.

The friction coefficient of all interfaces is assumed equal to 0.80 (Table 5). This value is higher than what usually assumed in technical standards, but rather close to the 0.79 mean value available in Marques (2021), related to brickwork laid in a natural hydraulic mortar. Classic manuals suggest similar values, for instance: Coulomb (1776) 0.75, Navier (1826) up to 0.81, Breymann (1885) 0.76. In the sensitivity analyses performed for the post-dictions a more conservative 0.60 value will be considered.

The elastic properties of masonry blocks, beams and lintels are reported in Table 6 and are derived from Table 1 whenever applicable. Finally, a 5% damping coefficient is assumed for all materials. Based on considerations developed by Galvez et al. (2022), the damping coefficient is proportional to stiffness.

4 Numerical results

4.1 Quantitative comparison of experimental results with simulations

The blind prediction was performed by means of the numerical model under the programmed testing sequence described in Table 2. The dynamic interaction between the two building units was evident in the time histories of the motion along the Y and X directions (Fig. 6). The simulations highlighted that the joint between the two building units opened very markedly (Fig. 6a), although with limited residual value until Run B3.3, the last significant one before the experimental tests were stopped (see Table 4). In Fig. 6a the one-sided nature of the relative displacement between the two building units is evident. Along the X direction the relative displacement is more symmetric and involves significant residual offsets in runs B4.2 and B4.3 (Fig. 6b).

A quantitative comparison between the numerical predictions (model Pre), when applicable (see Table 4), and the experimental results derived from Tomić et al. (2022b) is shown in Figs. 7, 8 and 9, where the sequence of the experimental runs is reported

on the ordinates. (The same figures show the comparison with the post-dictions, which will be discussed later). Displacements are presented in a logarithmic scale, given the very large difference between experimental values and some of the numerical values. In fact, displacement predictions largely overestimate the observed values, especially for run B1.3 (to be compared with E1.3) suggesting that the masonry stiffness is underestimated. The following runs, B3.1 (to be compared with E2.1) and B3.2 (to be compared with E2.2S), present displacements that are closer but still two-, four-times larger than the measured ones, regarding peak roof displacement, and six-, eight-times regarding peak interface openings. Base shear is largely underestimated, especially for the most severe runs.

Numerical post-dictions were performed considering seven models, whose main features are summarised in Table 7. The results of some post-dictions, along with their quantitative comparisons with the experimental results and the predictions, are presented in Figs. 7, 8 and 9. Therein, models Post5 and Post6 are omitted because less significant and in order to improve readability. Nonetheless, comments are given for all models.

Model Post1 presents the same characteristics of the model used for predictions but, as all post-dictions models, is excited by the actual shake-table motion (Table 3). When considering the peak roof displacements (Fig. 7), model Post1 has a better agreement than predictions, regarding both the runs and the specific quantities in Table 4 and comparing the average of all runs (Table 3). This agreement highlights the deviation of the actual ground motion from that assumed in predictions, also bearing in mind that a different motion sequence induces a different damage accumulation. Nonetheless, the mean of peak displacements of all runs is overestimated by a factor on average equal to about 5. The post-dictions of peak interface openings are improved compared to the predictions but are still overestimated by a factor on average equal to about 12 (Fig. 8). Finally, the post-dictions of peak base shear are less accurate in the early runs, while in the most severe tests they are rather close to the observed values (Fig. 9).

Based on experimental results, wherein no significant sliding was observed between timber and masonry, model Post2 has the interfaces between beams and blocks equal to those between blocks ($NFLS=170$ kPa). Peak roof displacements of all runs are overestimated by an average factor slightly smaller than that of model Post1. Peak interface openings are markedly improved compared to both Pre and Post1 models, although still overestimated by a mean factor of about 5. Peak base shear assessment is slightly improved compared to previous post-diction.

To simulate the strengthening intervention a third model, Post3, presents rigid beams as well as rigid interfaces between beams and blocks (lintels are unchanged). These modifications are applied since the first run and not at run E2.1S when strengthening was actually performed. This model has absolutely no benefit compared to the previous versions, regarding response quantities and damage prediction, as will be discussed in the following section. Peak roof displacement is overestimated by an average factor of 12, interface opening by an equivalent factor of 40, and base shear is underestimated by a mean factor of 0.8.

To pursue a reduction of elastic displacements, in model Post4 the Young's modulus of the blocks is equal to ten times that in previous models, while beam-block interface has a finite strength as in model Post2. Mean of peak roof displacements is overestimated by just about 10% compared to experimental ones. Additionally, the coefficient of variation of individual peak values is smaller for model Post4 compared to the second-best solution, model Post2. Peak interface openings are dramatically reduced compared to this model, and on average underestimated by a factor of about 0.6. Peak base shear assessment is slightly worsened compared to Post2 and equal to about 2.5. Hence, all these measures

considered, this model has the overall best performance. Unfortunately, the increased stiffness involves an integration step shorter by about 40% compared to previous versions, with a consequent additional computational burden.

Given the overestimation of base shear and (although slight), of roof displacement, a model with an increased Young's modulus (as in Post4), as well as simulated interventions (as in Post3) was implemented with the id Post5. The model has a much better performance than that of model Post3, but in general worse than that of model Post4. Even considering the first three runs and peak roof displacement, the overestimation factor is about 4.4, compared to 1.4 from model Post4. Interface displacements are overestimated by an average factor of 10, and base shear assessment is again worse than in model Post4. Hence, the changes to beams deliver again no advantage.

To investigate a more conservative value of the friction coefficient model Post6, equal to model Post4 but with friction coefficient reduced to 0.60, was implemented. Whereas mean numerical interface displacements are a better approximation of experimental values by 3% compared to model Post4, mean of peak roof displacements is overestimated by about 20% and mean of peak base shears is overestimated by about 10%. Hence, the 0.80 value assumed for model Post4 is more appropriate in the case at hand.

Finally, starting again from mechanical properties of model Post4, a block cubic discretisation is considered in model Post7 (Fig. 10). Number of blocks is substantially increased to 4297, almost three times those of previous models, while the number of FEs is only marginally enlarged. However, the reduction of the size of the smallest FE, combined with a much larger number of interfaces, involved an almost doubled time of analysis. Mean of peak roof displacements is overestimated by about 60% compared to experimental ones. Peak interface openings on average underestimated by a factor of about 0.8. Peak base shear assessment is equal to about 2.5 the experimental one. Hence, the overall performance is similar, or slightly worse, that of model Post 4 but at the price of a much more demanding computational time.

In addition to peak simulations, it is worth to analyse some time histories. In Figs. 11, 12 and 13 time histories of roof displacements, interface openings and base shear are shown, based on a selection accounting for excitation and instrumentation directions (Table 3; Fig. 4), with reference to sample runs E2.1, E2.1S and E2.2S, not necessarily the most effectively reproduced but those discussed in the following section based on

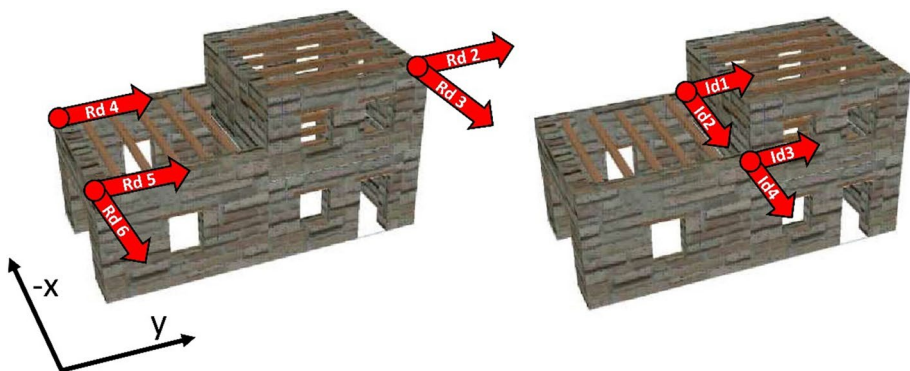


Fig. 4 Monitored relative displacements used in comparisons between simulations and experimental results. Rd=roof displacement relative to table, Id=interface opening, i.e. Unit 2 displacement relative to Unit 1 (adapted after Tomić et al. 2022a)

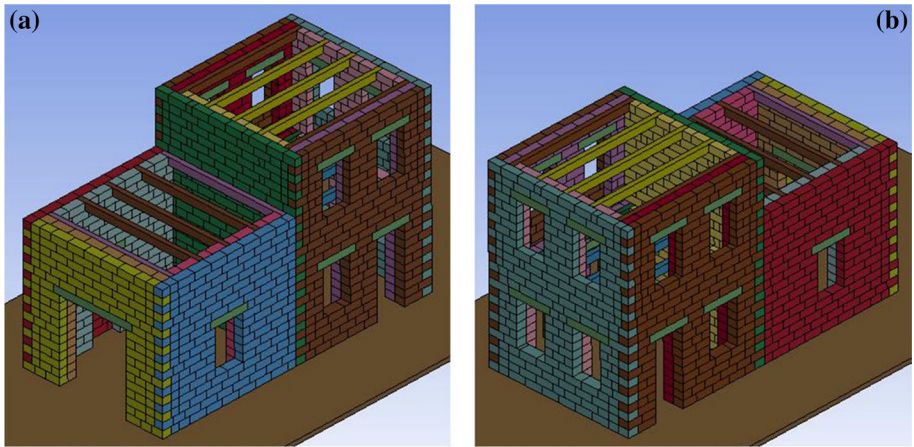


Fig. 5 FEM-DEM numerical model for blind predictions: **a** facades 1, 3 and 5 are visible; **b** facades 2 and 4 are visible. Discrete elements are coloured only for presentation purposes, their material properties being homogeneous

Table 5 Numerical model interface parameters for blind prediction

Parameter	Interface between blocks, interface between lintel and block	Interface between building units, interface between beam and block
Normal failure limit stress; <i>NFLS</i> [kPa]	170	0.1
Shear failure limit stress; <i>SFLS</i> [kPa]	233	233
Static, Dynamic friction coefficient; <i>FS</i> , <i>FD</i> [-]	0.8	0.8

Table 6 Numerical model material properties for blind prediction

Parameter	Block	Beam, lintel
Density; ρ [Mg/m ³]	1.980	0.825
Young's modulus; <i>E</i> [GPa]	3.462	12.000
Poisson's ratio; ν [-]	0.140	0.200

available damage documentation. Ordinates are zoomed in on experimental values to get a more detailed portrayal, given that maximum simulation values were already presented in Figs. 7, 8 and 9.

Time history displacement prediction is rather poor, in terms of both sign and time of occurrence of maxima, overall waveform shape and residual offset (Fig. 11). Multiple interface openings are predicted (Fig. 12), larger or smaller depending on the model, while experimental counterparts are fewer in peaks. Preliminary simulations, not shown here for the sake of conciseness, assuming damping proportional both to mass and stiffness, or

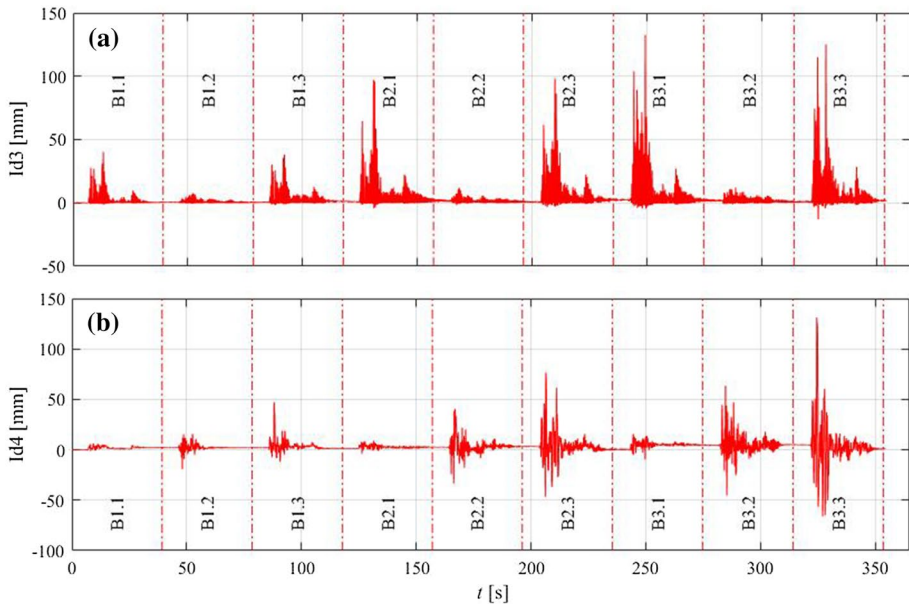


Fig. 6 Blind prediction time histories of the opening of the interface between the two building units: **a** Y direction; **b** X direction. Identification of measured displacements as in Fig. 4

Table 7 Features of numerical models for post-dictions, all excited by actual shake table motion. Model relevant changes relative to previous version are in boldface. All other parameters as in Tables 5 and 6

Model	Interface between beam and block; $NFLS$ [kPa]	Beam	Young's modulus; E [GPa]	Friction coefficient; FS, FD [-]	Block geometry
Post1	0.1	Elastic	3.462	0.8	parallelepiped
Post2	170	Elastic	3.462	0.8	parallelepiped
Post3	rigid	Rigid	3.462	0.8	parallelepiped
Post4	170	Elastic	34.62	0.8	parallelepiped
Post5	rigid	Rigid	34.62	0.8	parallelepiped
Post6	170	Elastic	34.62	0.6	parallelepiped
Post7	170	Elastic	34.62	0.8	cubic

with a larger damping coefficient, did not improve markedly the results. Base shear predictions in Fig. 13 are in better agreement, compared to the previous plots, as could also be expected from peak values in Fig. 9. Both displacement and shear experimental values showed very little coupling between horizontal components, meaning that when the specimen was excited along the Y direction the response along X was very small. This behaviour is not observed in numerical simulations, wherein a non-negligible response was measured along the direction normal to that of the excitation. A possible explanation is that the comparatively large size of the blocks and their regular shape delivered a corner interlocking

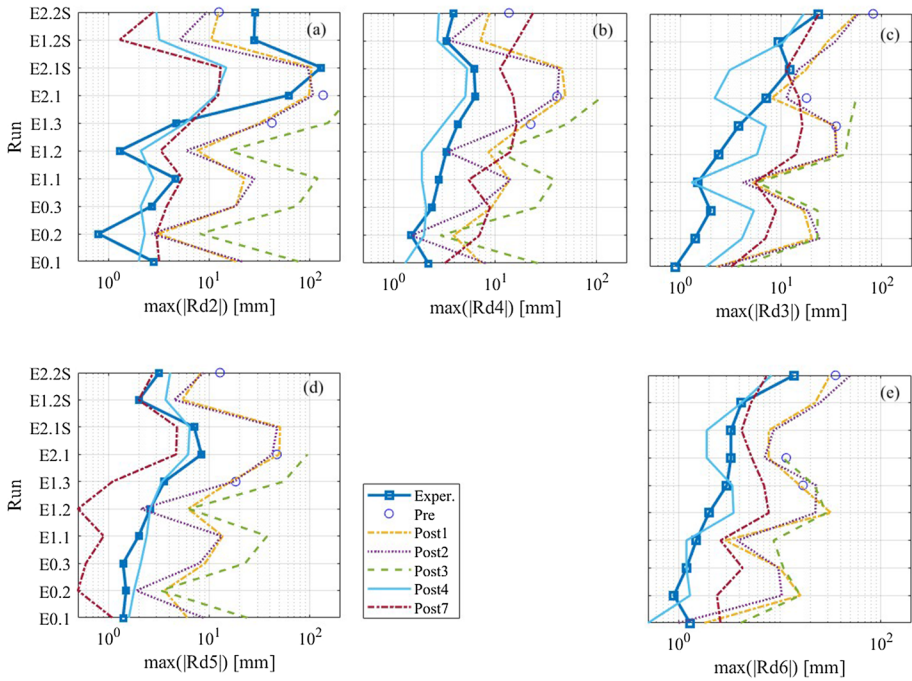


Fig. 7 Comparison of maximum experimental results with blind predictions (when applicable) and selected post-dictions. Roof displacement (Fig. 4): **a, b, d** along *Y* direction, **c** and **e** along *X* direction

still more effective than in reality, despite the low number of interlocking units shown in Fig. 5.

4.2 Qualitative description of the damage mechanisms

Damage progression, as reported by Tomić et al. (2022b), is summarised in Fig. 14 for three specific runs, wherein red lines are related to cracks occurring at that run and black lines are related to damage corresponding to previous runs. In the following, these crack maps are compared with the deformation axonometric views of the corresponding simulations, adapting the displacement scale factor (SF) to the severity of response for an improved readability. Additionally, colourmaps of six steps of horizontal displacement (relative to shake table) are used in the following figures, resorting to different scales to account for differences in response severity. Therefore, in each caption the minimum displacement (MD) and the displacement colour step (DCS) of each run are reported.

Based on Table 4, in Fig. 15 the blind predictions are shown for two runs only. For run B3.1 (Fig. 15a), to be compared with run E2.1 (Fig. 14a), the piers of the upper story of Unit 2 belonging to Facade 2 and Facade 3 are greatly engaged, especially that between the windows of Facade 2. The out-of-plane response of the upper story is captured as well. Hence, numerical results and laboratory tests are in reasonable agreement, although the unseating of some beams was not observed in the laboratory. Similarly, the lower story does not show any significant damage in the numerical simulations, whereas some cracks can be noticed in Fig. 14a. As for run B3.2, the response in Fig. 15b is significantly

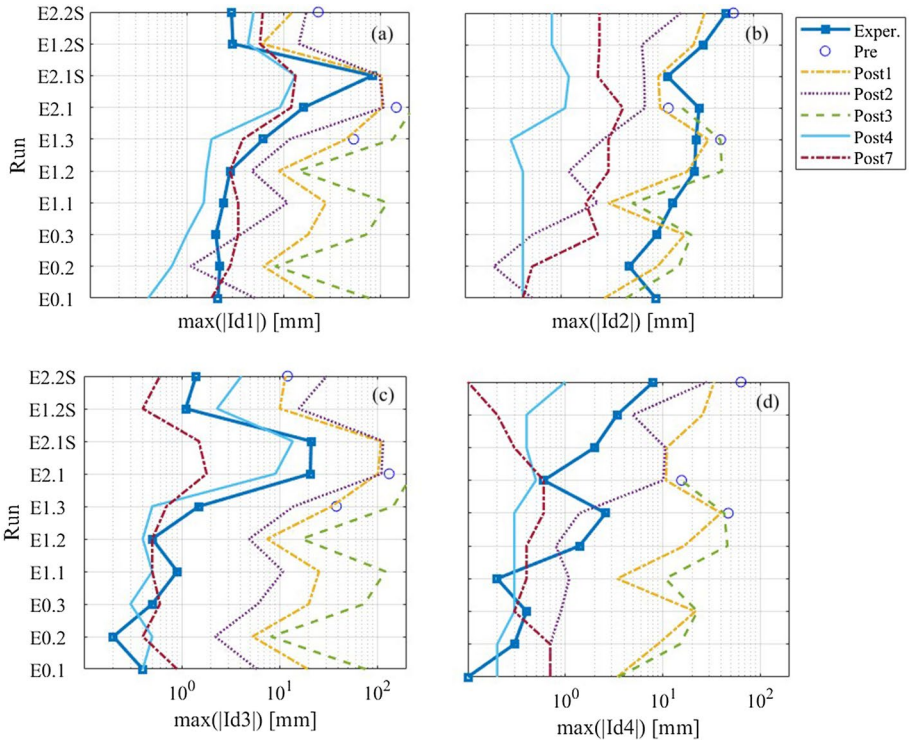


Fig. 8 Comparison of maximum experimental results with blind predictions (when applicable) and selected post-dictions. Interface opening (Fig. 4): **a** and **c** along Y direction, **b** and **d** along X direction

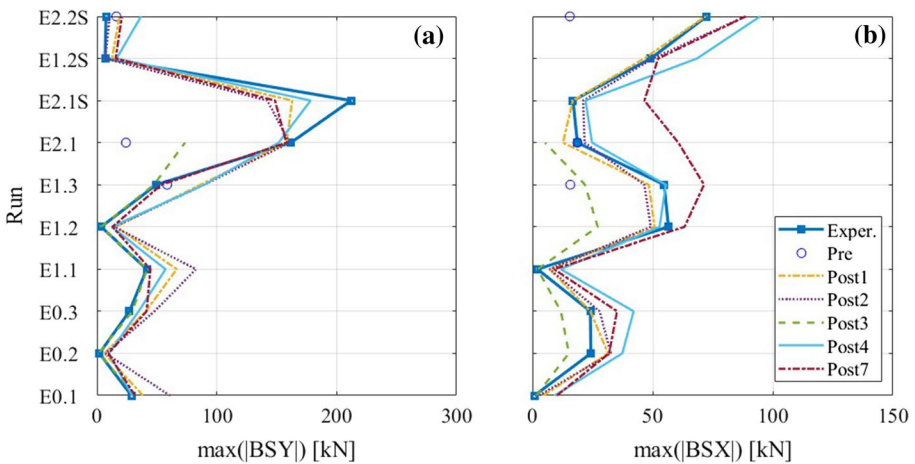


Fig. 9 Comparison of maximum experimental results with blind predictions (when applicable) and selected post-dictions. Base shear: **a** Y direction, **b** X direction

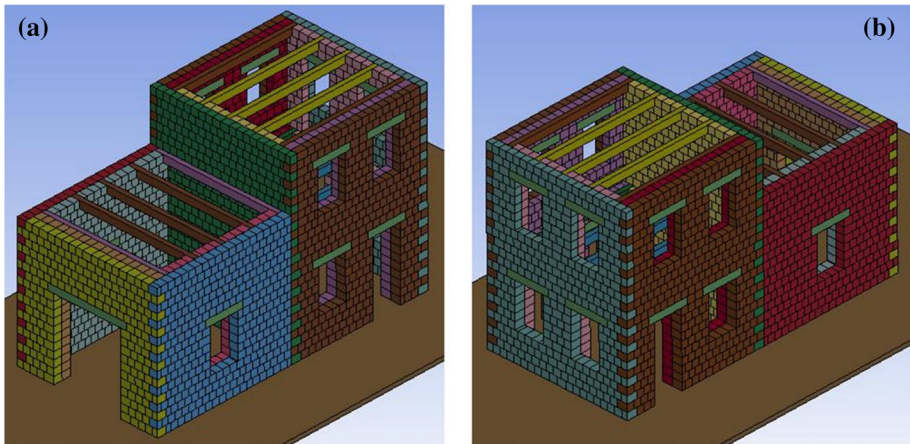


Fig. 10 FEM-DEM element numerical Post7 model: **a** facades 1, 3 and 5 are visible; **b** facades 2 and 4 are visible. Discrete elements are coloured only for presentation purposes, their material properties being homogeneous

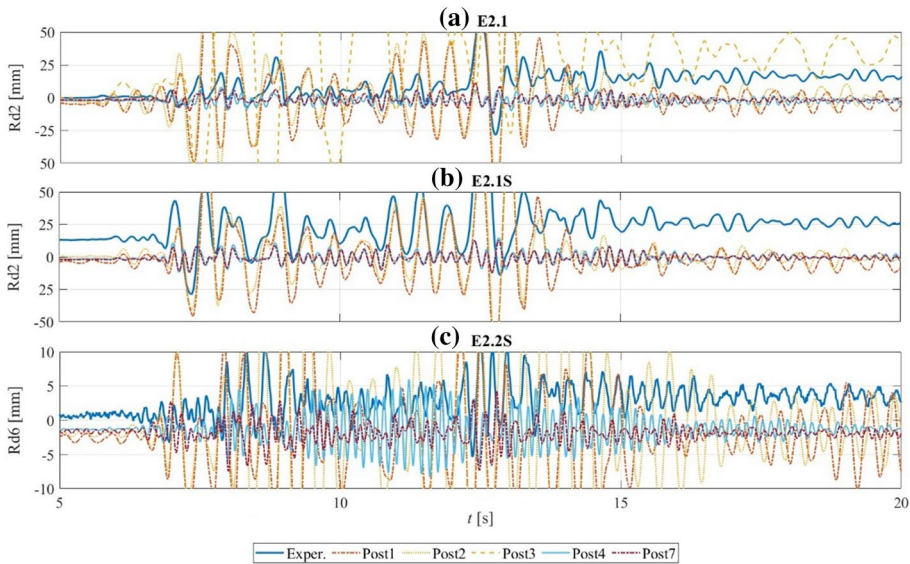


Fig. 11 Sample experimental and numerical time histories of roof displacement (Table 3; Fig. 4): **a** run E2.1, **b** run E2.1S, **c** run E2.2S

different from that in Fig. 14c, run E2.2S. Although Unit 1 is the most engaged in these two cases, the numerical response is dominated by the opening of the interface and by a torsional response due to the lack of an interlocked wall close to Unit 2, while the experimental response shows only some cracks in Facade 1. The overall prediction of the experimental damage pattern can be considered reasonable. Extensive damage (overturning of facades 2, 3 and 4, involving the collapse of the roof of the tallest building unit) occurred

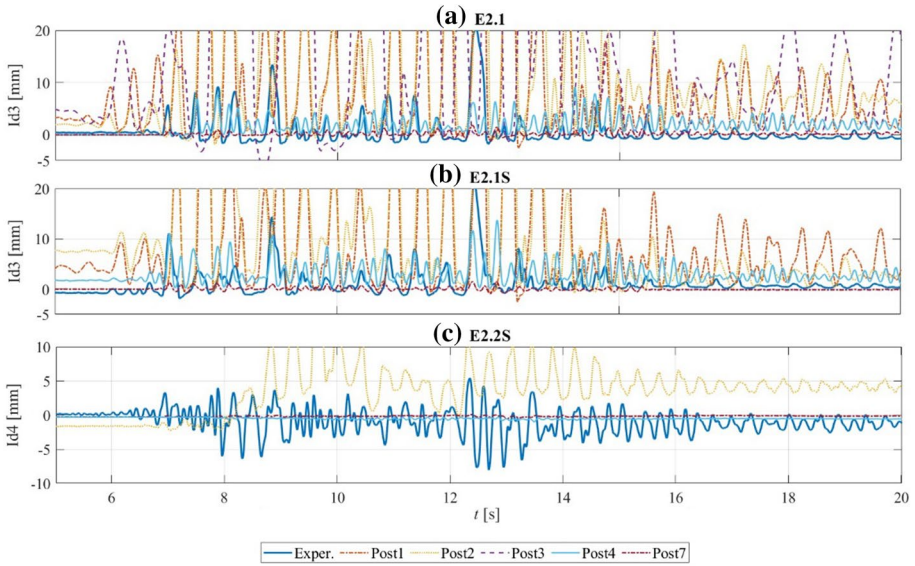


Fig. 12 Sample experimental and numerical time histories of interface openings: **a** run E2.1, **b** run E2.1S, **c** run E2.2S

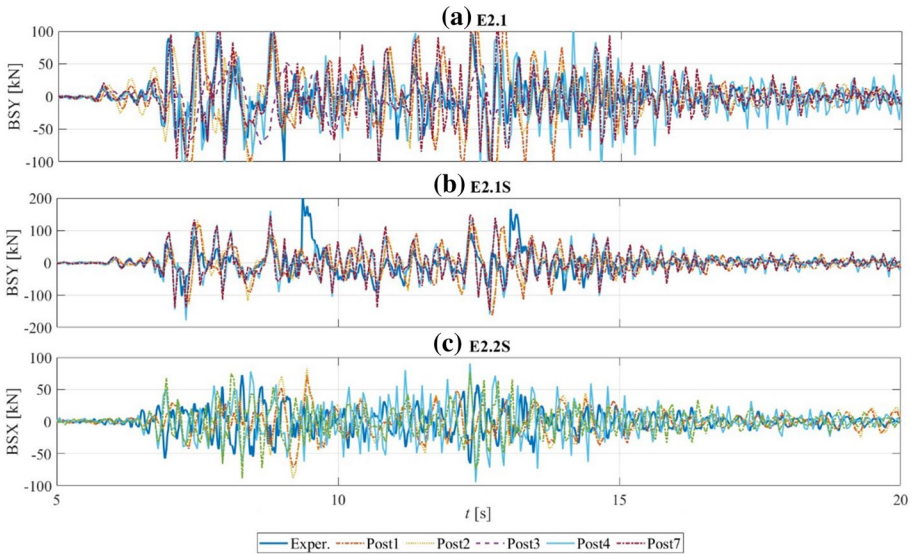


Fig. 13 Sample experimental and numerical time histories of base shear: **a** run E2.1, **b** run E2.1S, **c** run E2.2S

in the blind predictions in following runs, for a level of shaking not tested to avoid damage to laboratory facilities.

Simulations of model Post1 are presented in Fig. 16, showing a lighter damage level at the upper storey when compared to blind predictions, but better capturing damage at

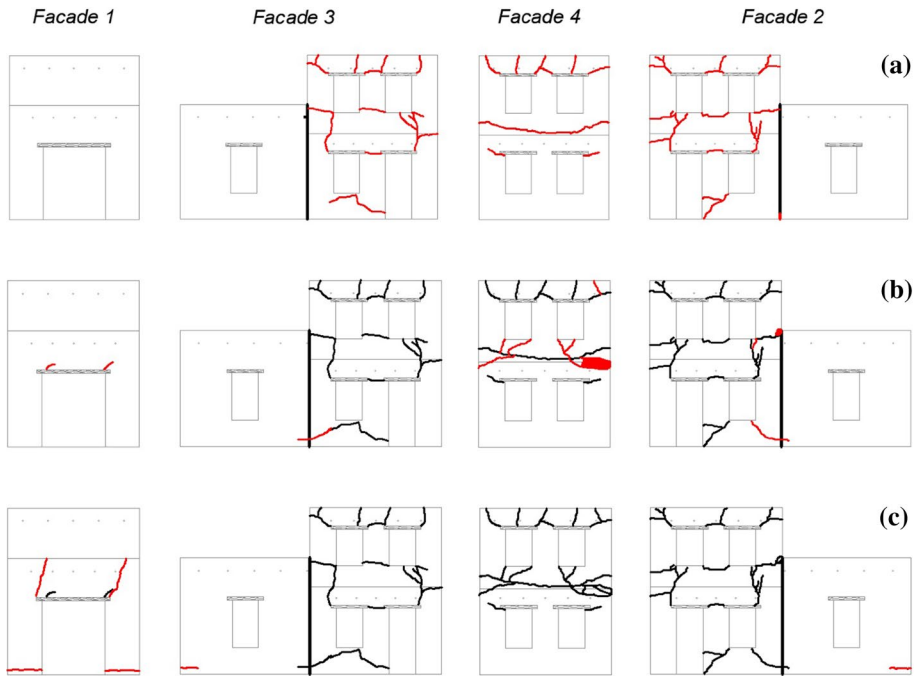


Fig. 14 Experimental crack maps at the end of: **a** run E2.1, **b** run E2.1S, **c** run E2.2S (adapted after Tomić et al. 2022b)

the lower storey. The separation at cold joint is clearly visible in the analysis step shown in the figure. In the following run (Fig. 16 b), Facade 4 is more engaged than in previous runs, in reasonable agreement with the observed behaviour. Along the X direction (Fig. 16c) the response is like that described with reference to predictions. The unseating of some beams can still be observed, thus suggesting the adoption of an improved contact between timber and masonry.

The enhanced connection of beams on blocks avoids the unseating of the beams of Unit 2 in model Post2 (Fig. 17). However, the damage pattern on masonry walls is like that of the model Post1.

Run E2.2S was performed after the activation of the steel anchors between beams and walls. This condition was approximately simulated, from the very beginning, in model Post3 and it triggers a premature collapse during run E2.1 (Fig. 18), thus suggesting that the introduction of rigid elements can unpredictably affect the response and should be carefully considered.

The overall over-prediction of displacements suggested an increased elastic modulus, implemented in model Post4 (Fig. 19) and requiring an increased SF for the displacements. The smaller engagement of the cold joint between the building units is evident, but pounding is still accounted for. Damage is more evident at spandrels of Facade 2 and Facade 3, but the activation of the in-plane rocking of the piers between the opening is still recognizable. For an easier identification of the interfaces that opened during the runs, numerical crack maps are presented in Fig. 20. They can be compared with experimental ones in Fig. 14, highlighting that in run E2.1 the sub-horizontal crack at

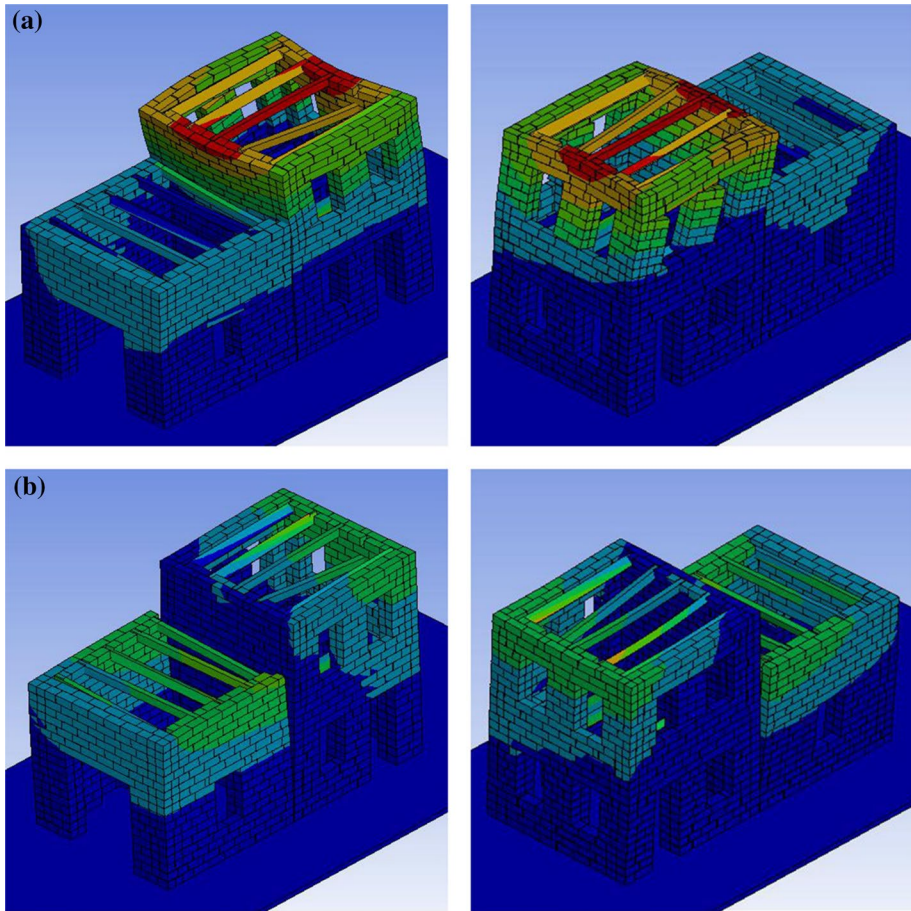


Fig. 15 Horizontal displacement colour contours superimposed on model Pre deformation at significant point in time: **a** run B3.1 (MD: -4 mm, DCS: 25 mm), to be compared with run E2.1; **b** run B3.2 (MD: 0 mm, DCS: 15 mm), to be compared with run E2.2S (Table 4). (SF=3)

mid-height of Facade 4 is not predicted, while the overall damage pattern of Facade 2 and Facade 3 is reasonably reproduced.

In run E2.1S the experimental damage is concentrated at the horizontal central band of Facade 4, which again escapes the numerical simulation. The cracks in the upper portion of the same facade and at the base of Facade 3 are better predicted. In run E2.2S, with shake-table motion along the X direction, the substantial damage of Facade 1 is only partially reproduced. No new experimental crack affects Facade 4, while those appearing in the numerical simulation bring the overall map closer to final laboratory one.

The combinations of models Post3 and Post4 in model Post5 involves a more marked concentration of damage at the lower storey because of increased horizontal accelerations and base shear (Fig. 21). Model Post6, with a reduced friction coefficient compared to model Post4, has an overall damage distribution (Fig. 22) very similar to that of its reference version, and displacement values are reasonably close too. Model Post7 (Fig. 23), with cubic blocks, shows a damage pattern like that of model Post 4, of which it shares the

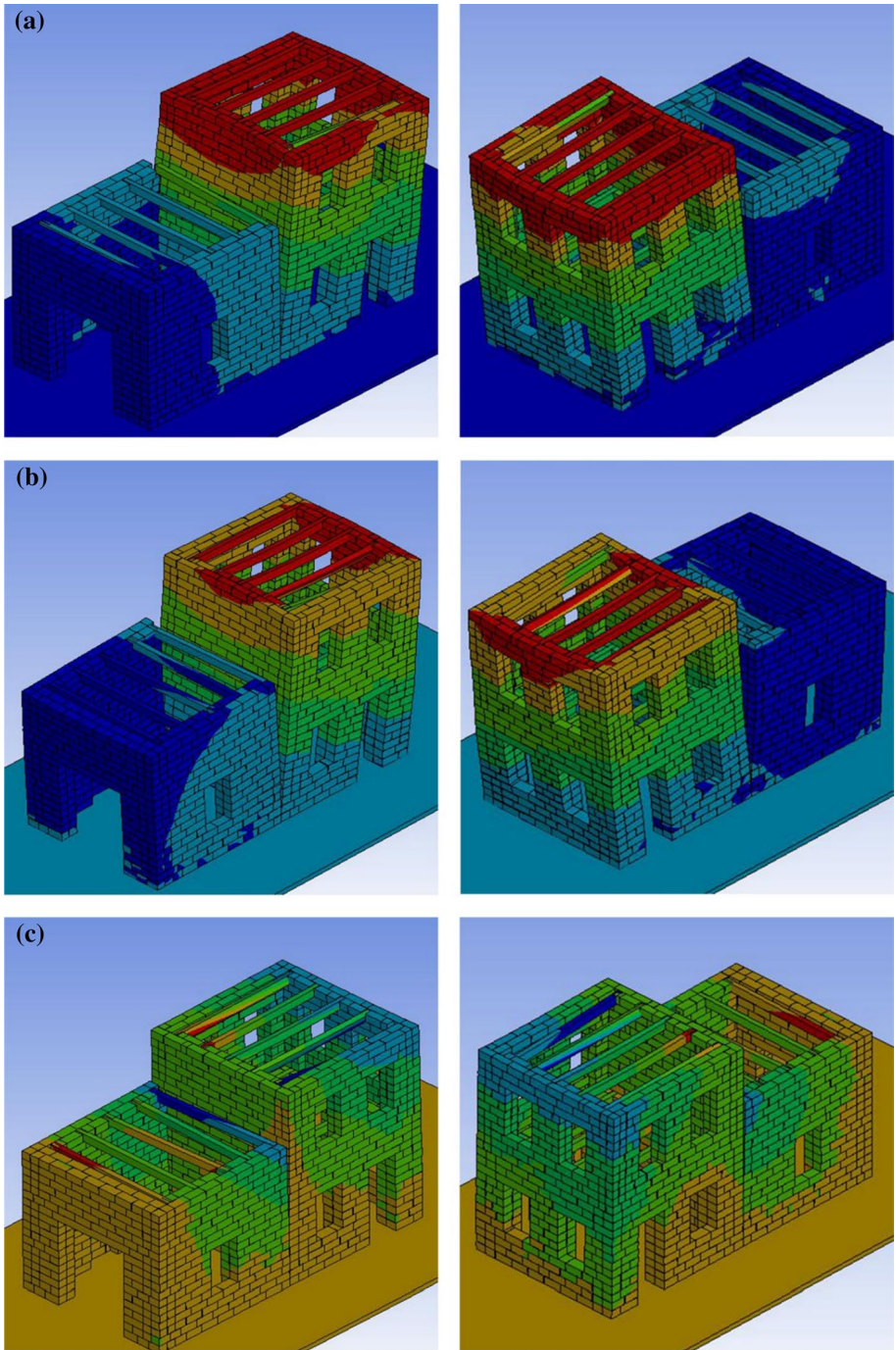


Fig. 16 Horizontal displacement colour contours superimposed on model Post1 deformation at significant point in time: **a** run E2.1 (MD: -10 mm, DCS: 10 mm); **b** run E2.1S (MD: -10 mm, DCS: 10 mm); **c** run E2.2S (MD: -10 mm, DCS: 10 mm). (SF=3)

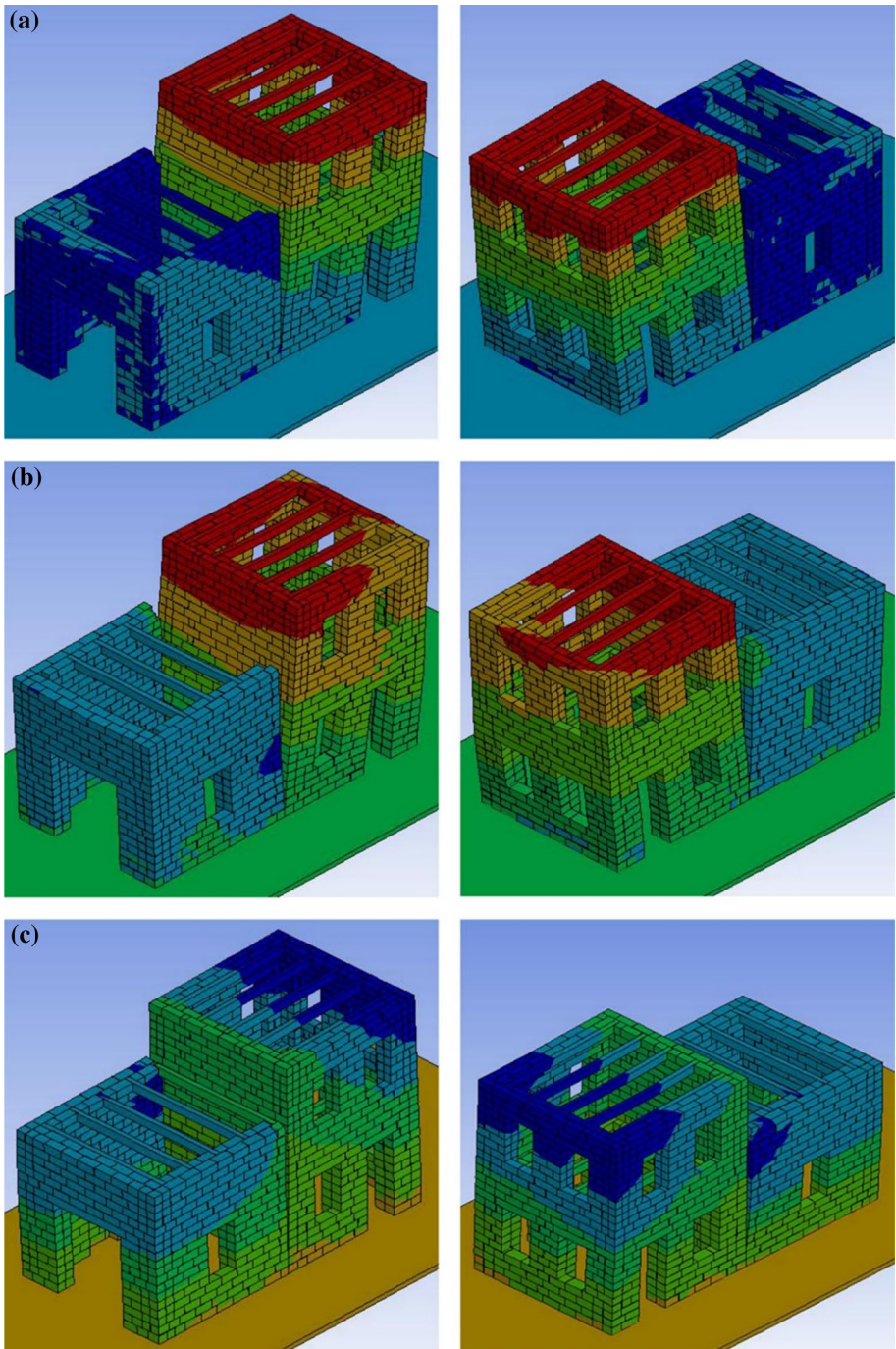


Fig. 17 Horizontal displacement colour contours superimposed on model Post2 deformation at significant point in time: **a** run E2.1 (MD: -10 mm, DCS: 10 mm); **b** run E2.1S (MD: -20 mm, DCS: 10 mm); **c** run E2.2S (MD: -40 mm, DCS: 10 mm). (SF=3)

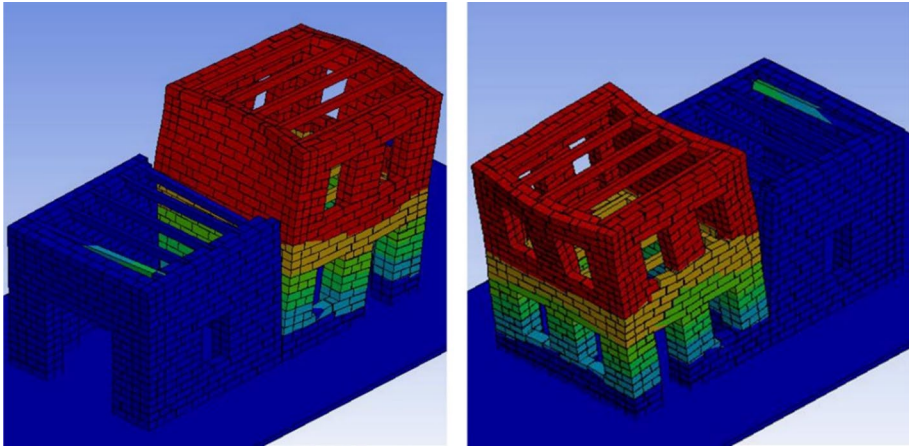


Fig. 18 Horizontal displacement colour contours superimposed on model Post3 deformation at significant point in time: run E2.1 (MD: -4 mm, DCS: 10 mm). (SF=3)

same mechanical parameters. The shorter units involve a somewhat more distributed deformation but without dramatic differences.

5 Conclusion

Building aggregates account for most of the unreinforced masonry constructions of historical centres and frequently present a poor earthquake performance. However, no established modelling and assessment procedures exist, and this topic has attracted so far limited attention in the scientific literature. To fill this gap, an experimental campaign was designed and performed by other Authors within the Seismology and Earthquake Engineering Research Infrastructure Alliance for Europe (SERA), and specifically within the Seismic Testing of Adjacent Interacting Masonry Structures (AIMS) program. In this paper the physical building aggregate made of two non-interlocked building units is modelled resorting to a finite element method - discrete element method (FEM-DEM) approach and non-linear dynamic analyses are performed both as blind prediction and as post-diction simulations. The FEM-DEM model accounts jointly for the in-plane and the out-of-plane response of the walls. Moreover, the interfaces between the blocks used to discretise the masonry can crack, allowing sliding, as well as complete separation. Additionally, such an interface with very weak tensile strength is used at the cold joint between the two building units.

Blind predictions, according to the scheduled testing sequence, show the clear separation and pounding between the two building units, a phenomenon never modelled previously in the literature. Peak displacements are largely overpredicted with reference to comparable experimental runs, whereas peak base shear is underpredicted. Damage pattern is in reasonable agreement with the observed response, except for beams that are unseated in the FEM-DEM model, whereas no such response was observed in the laboratory.

Simulations are repeated using the same model but the actual testing sequence (Post1). Quantitative simulations are slightly improved for displacements and markedly improved for base shear, while damage estimate is rather like predictions, including beam unseating. Therefore, several sensitivity analyses are performed. A model (Post2) presenting a

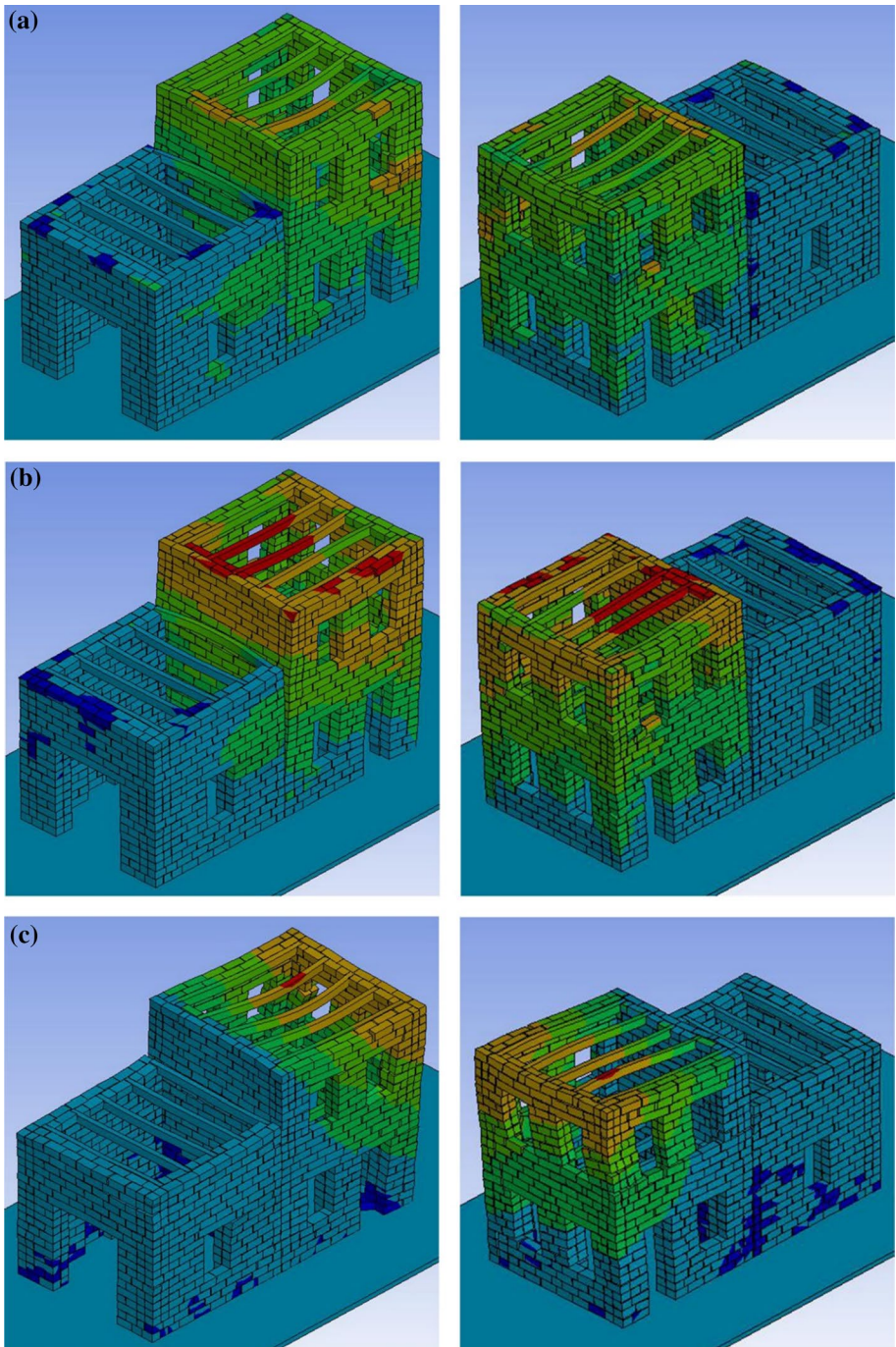


Fig. 19 Horizontal displacement colour contours superimposed on model Post4 deformation at significant point in time: **a** run E2.1 (MD: -1.0 mm, DCS: 1.5 mm); **b** run E2.1S (MD: -2.0 mm, DCS: 2.0 mm); **c** run E2.2S (MD: -4.0 mm, DCS: 5.0 mm). (SF = 15)

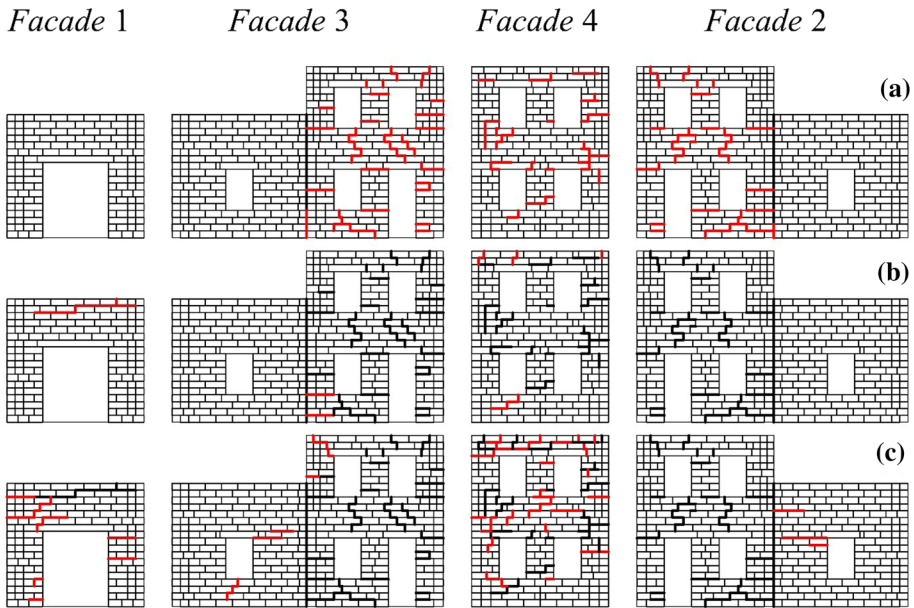


Fig. 20 Numerical crack maps of model Post4 at the end of: **a** run E2.1, **b** run E2.1S, **c** run E2.2S

beam-block interface equal to the block-block interface is implemented and analyses are repeated. Quantitative peak displacement predictions are markedly improved, although still largely overestimating experimental values.

To approximately simulate the connection between floors and walls, rigid interfaces and beams are considered in model Post3 from the first experimental run. The outcome is not encouraging because of the occurrence of a premature collapse.

To reduce displacement overestimation, Young’s modulus is increased by an order of magnitude in model Post4, starting from model Post2. An overall marked improvement is obtained, delivering the best post-diction. Combining rigid beam-block interface and rigid beams with increased Young’s modulus (Post5) or considering a more conservative value of the friction coefficient (Post6) does not improve the simulations. A cubic discretisation of the masonry (Post7) delivers results similar to that of the reference model (Post4) but with an almost doubled computation time.

In summary, advantages and disadvantages, as well as substantial challenges, are associated with the FEM-DEM approach. On the positive side, it can account for several phenomena neglected by other non-linear dynamic strategies such as: combined in-plane and out-of-plane response of walls, failure of wall-to-wall and floor-to-wall connections, pounding between adjacent building units, possible disintegration of wall section. However, computational cost is very large and to keep it reasonable very small or irregular blocks need to be avoided. Moreover, several choices need to be picked in the modelling phase, regarding geometric bond pattern, block size and material properties, while clear indications are still missing. FEM-DEM modelling can deliver a reasonable quantitative prediction even of rather large displacements provided that the Young’s modulus is properly selected. On the contrary, at least in the case at hand and in the investigated range, sensitivity to friction coefficient value seems limited. The assessment of damage pattern and overall capacity of the structure are less sensitive to mechanical parameters, provided that

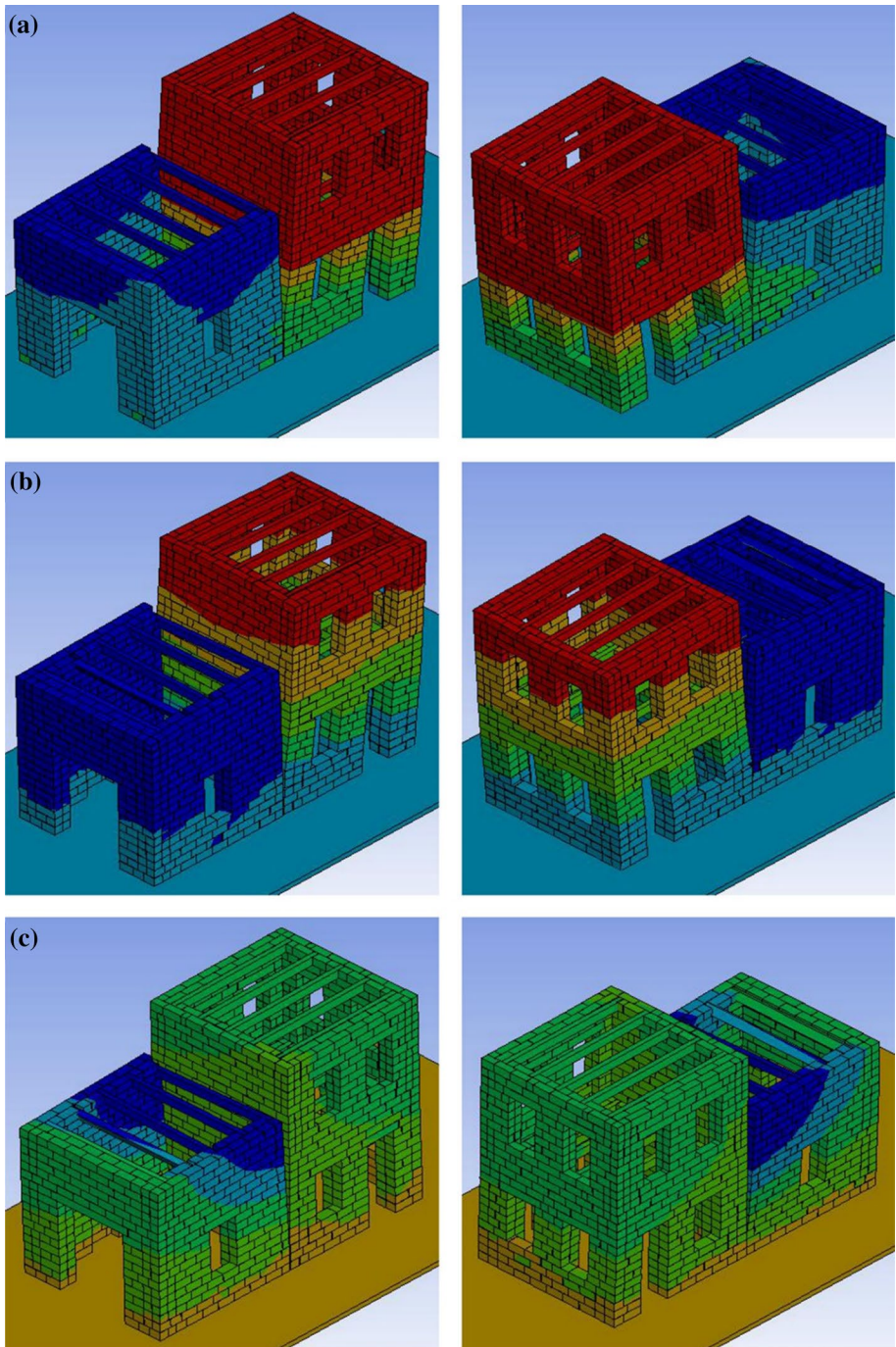


Fig. 21 Horizontal displacement colour contours superimposed on model Post5 deformation at significant point in time: **a** run E2.1 (MD: -20 mm, DCS: 10 mm); **b** run E2.1S (MD: 0 mm, DCS: 10 mm); **c** run E2.2S (MD: -40 mm, DCS: 10 mm). (SF=3)

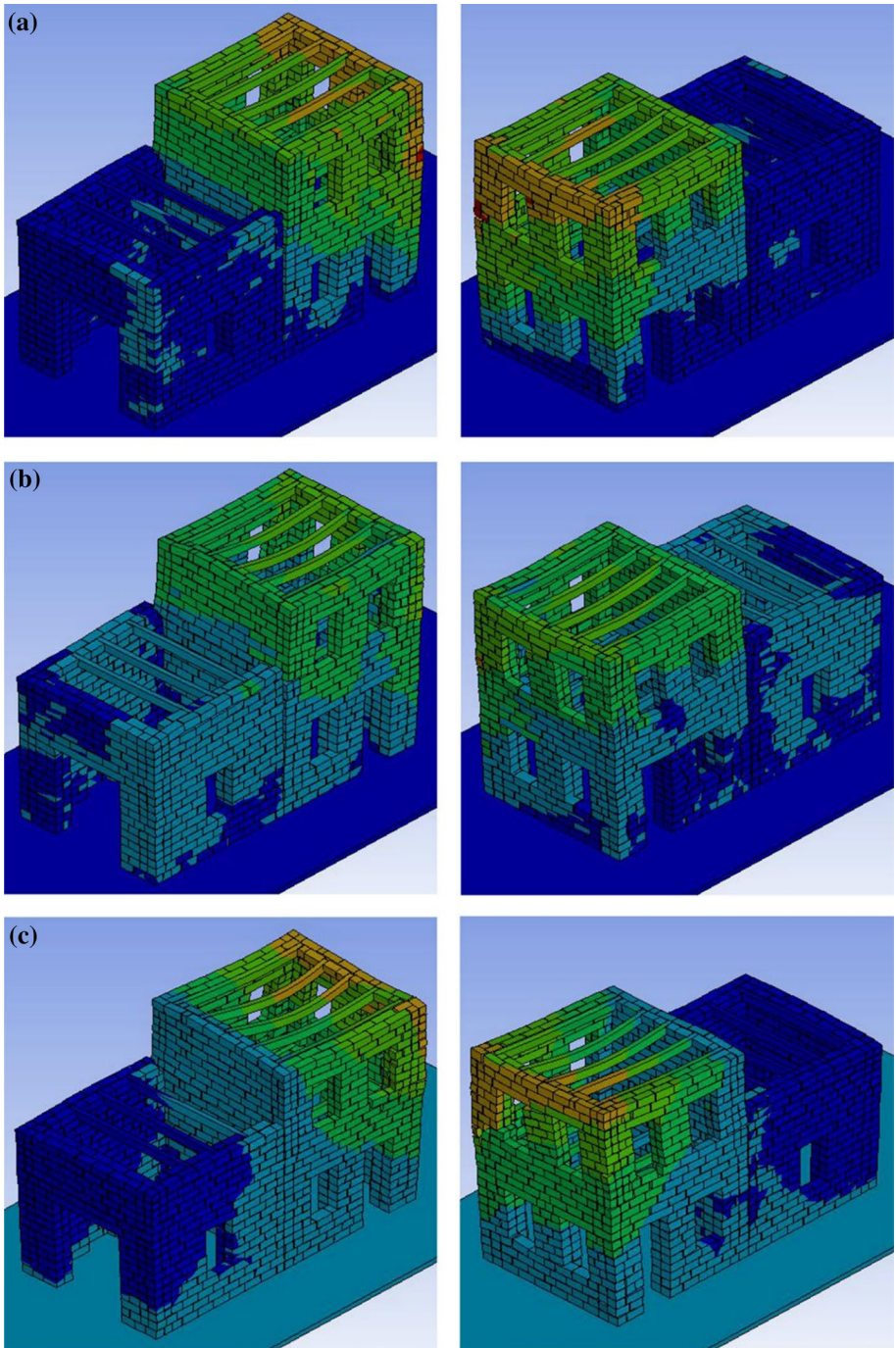


Fig. 22 Horizontal displacement colour contours superimposed on model Post6 deformation at significant point in time: **a** run E2.1 (MD: -1.0 mm, DCS: 1.5 mm); **b** run E2.1S (MD: -2.0 mm, DCS: 2.0 mm); **c** run E2.2S (MD: -4.0 mm, DCS: 5.0 mm). (SF = 15)

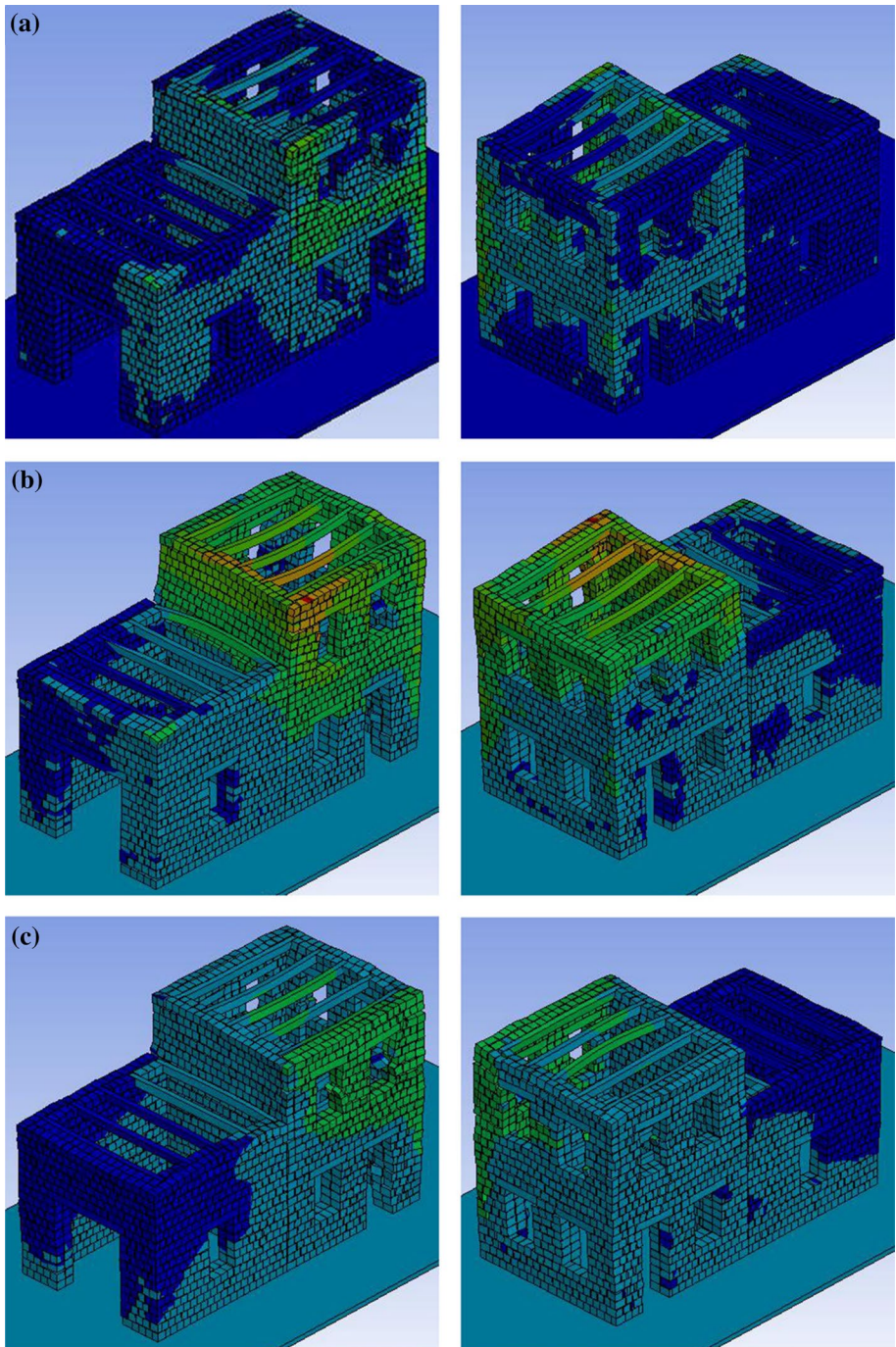


Fig. 23 Horizontal displacement colour contours superimposed on model Post7 deformation at significant point in time: **a** run E2.1 (MD: -1.0 mm, DCS: 1.5 mm); **b** run E2.1S (MD: -2.0 mm, DCS: 2.0 mm); **c** run E2.2S (MD: -4.0 mm, DCS: 5.0 mm). (SF = 15)

infinite strength connections are avoided. Finally, additional investigation is necessary to introduce strengthening interventions on a previously damaged model and in a way closer to actual structural details.

Acknowledgements This work was partially carried out within the research project ‘Damascus: Disintegration Analysis of MASony Constructions Under Seismic actions’ funded by Sapienza University of Rome, and partially funded by the ‘Dipartimento di Protezione Civile – Consorzio RELUIS’ program. The opinions expressed in this publication are those of the authors and are not necessarily endorsed by the funding bodies.

Funding Open access funding provided by Università degli Studi di Roma La Sapienza within the CRUI-CARE Agreement. This work was partially carried out within the research project ‘Damascus: Disintegration Analysis of MASony Constructions Under Seismic actions’ funded by Sapienza University of Rome, and partially funded by the ‘Dipartimento di Protezione Civile – Consorzio RELUIS’ program

Data availability The experimental data used in this article are those in Tomić et al. (2022b).

Declarations

Competing interests The authors declare no competing interest, financial or otherwise.

Open Access This article is licensed under a Creative Commons Attribution 4.0 International License, which permits use, sharing, adaptation, distribution and reproduction in any medium or format, as long as you give appropriate credit to the original author(s) and the source, provide a link to the Creative Commons licence, and indicate if changes were made. The images or other third party material in this article are included in the article’s Creative Commons licence, unless indicated otherwise in a credit line to the material. If material is not included in the article’s Creative Commons licence and your intended use is not permitted by statutory regulation or exceeds the permitted use, you will need to obtain permission directly from the copyright holder. To view a copy of this licence, visit <http://creativecommons.org/licenses/by/4.0/>.

References

- Abrams DP, AlShawa O, Lourenço PB, Sorrentino L (2017) Out-of-plane seismic response of unreinforced masonry walls: conceptual discussion, research needs, and modeling issues. *Int J Archit Herit* 11:22–30. <https://doi.org/10.1080/15583058.2016.1238977>
- AlShawa O, Sorrentino L, Liberatore D (2017) Simulation of shake table tests on out-of-plane masonry buildings. part (II): combined finite-discrete elements. *Int J Archit Herit* 11:79–93. <https://doi.org/10.1080/15583058.2016.1237588>
- Breymann GA (1885) *Trattato generale di costruzioni civili con cenni speciali intorno alle costruzioni grandiose, Costruzioni in pietra e strutture murali*. Vallardi, Milano
- Carocci CF (2012) Small centres damaged by 2009 L’Aquila earthquake: on site analyses of historical masonry aggregates. *Bull Earthq Eng* 10:45–71. <https://doi.org/10.1007/s10518-011-9284-0>
- Cocco G, D’Aloisio A, Spacone E, Brando G (2019) Seismic vulnerability of buildings in historic centers: from the “urban” to the “aggregate” scale. *Front Built Environ* 5:78. <https://doi.org/10.3389/fbuil.2019.00078>
- Coulomb CA (1776) *Essai sur une application des règles de maximis et minimis à quelques problèmes de statique. Mémoires mathématiques Phys présentés à l’académie R des Sci par Divers savants lus dans les Assem 7*
- da Porto F, Munari M, Prota A, Modena C (2013) Analysis and repair of clustered buildings: Case study of a block in the historic city centre of L’Aquila (Central Italy). *Constr Build Mater* 38:1221–1237. <https://doi.org/10.1016/j.conbuildmat.2012.09.108>
- D’Altri AM, Sarhosis V, Milani G et al (2020) Modeling strategies for the computational analysis of unreinforced masonry structures: review and classification. *Arch Comput Methods Eng* 27:1153–1185. <https://doi.org/10.1007/s11831-019-09351-x>
- de Felice G, Liberatore D, De Santis S et al (2022) Seismic behaviour of rubble masonry: Shake table test and numerical modelling. *Earthq Eng Struct Dyn* 51:1245–1266. <https://doi.org/10.1002/eqe.3613>
- Di Ludovico M, Digrisolo A, Graziotti F et al (2017) The contribution of ReLUIS to the usability assessment of school buildings following the 2016 central Italy earthquake. *Boll di Geofis Teor ed Appl* 58:353–376. <https://doi.org/10.4430/bgta0192>

- Flanagan DP, Belytschko T (1981) A uniform strain hexahedron and quadrilateral with orthogonal hourglass control. *Int J Numer Methods Eng* 17:679–706. <https://doi.org/10.1002/nme.1620170504>
- Formisano A, Florio G, Landolfo R, Mazzolani FM (2015) Numerical calibration of an easy method for seismic behaviour assessment on large scale of masonry building aggregates. *Adv Eng Softw* 80:116–138. <https://doi.org/10.1016/j.advengsoft.2014.09.013>
- Galvez F, Sorrentino L, Dizhur D, Ingham JM (2022) Damping considerations for rocking block dynamics using the discrete element method. *Earthq Eng Struct Dyn* 51:935–957. <https://doi.org/10.1002/eqe.3598>
- Grillanda N, Valente M, Milani G et al (2020) Advanced numerical strategies for seismic assessment of historical masonry aggregates. *Eng Struct* 212:110441. <https://doi.org/10.1016/j.engstruct.2020.110441>
- Hallquist J (2006) LS-DYNA theory manual. Livermore Software Technology Corporation, Livermore
- Ingham JM, Abeling S, Vallis S et al (2018) Seismic vulnerability assessment for precincts of unreinforced masonry buildings in New Zealand and Australia. In: Proceedings of the 10th International Masonry Society Conference. pp 29–56
- Liberatore D, Doglioni C, AlShawa O et al (2019) Effects of coseismic ground vertical motion on masonry constructions damage during the 2016 Amatrice-Norcia (Central Italy) earthquakes. *Soil Dyn Earthq Eng* 120:423–435. <https://doi.org/10.1016/j.soildyn.2019.02.015>
- Maio R, Vicente R, Formisano A, Varum H (2015) Seismic vulnerability of building aggregates through hybrid and indirect assessment techniques. *Bull Earthq Eng* 13:2995–3014. <https://doi.org/10.1007/s10518-015-9747-9>
- Malcata M, Ponte M, Tiberti S et al (2020) Failure analysis of a Portuguese cultural heritage masterpiece: Bonet building in Sintra. *Eng Fail Anal* 115:104636. <https://doi.org/10.1016/j.engfailanal.2020.104636>
- Marotta A, Goded T, Giovinazzi S et al (2015) An inventory of unreinforced masonry churches in New Zealand. *Bull New Zeal Soc Earthq Eng* 48:170–189. <https://doi.org/10.5459/bnzsee.48.3.170-189>
- Marques AI (2021) Shear test of masonry specimens. In: Lisbon Natl Lab Civ Eng <https://sera-crossvault.wixsite.com/blindprediction>. Accessed on 23 Aug 2022
- Mazzoni S, Castori G, Galasso C et al (2018) 2016–2017 Central Italy earthquake sequence: seismic retrofit policy and effectiveness. *Earthq Spectra* 34:1671–1691. <https://doi.org/10.1193/100717EQS197M>
- Navier LMH (1826) *Resumé des leçons données à l'École des Ponts et Chaussées sur l'application de la mécanique à l'établissement des constructions et des machines*. Paris: Firmin Didot, vol 1833, 2nd edn. Chez Carilian-Goeury, Paris
- Pujades LG, Barbat AH, González-Drigo R et al (2012) Seismic performance of a block of buildings representative of the typical construction in the Eixample district in Barcelona (Spain). *Bull Earthq Eng* 10:331–349. <https://doi.org/10.1007/s10518-010-9207-5>
- Roca P, Cervera M, Gariup G, Luca P (2010) Structural analysis of masonry historical constructions. Classical and advanced approaches. *Arch Comput Methods Eng* 17:299–325. <https://doi.org/10.1007/s11831-010-9046-1>
- Senaldi I, Magenes G, Penna A (2010) Numerical Investigations on the Seismic Response of Masonry Building Aggregates. *Adv Mater Res* 133–134:715–720. <https://doi.org/10.4028/www.scientific.net/AMR.133-134.715>
- Senaldi I, Guerrini G, Solenghi M et al (2019) Numerical modelling of the seismic response of a half-scale stone masonry aggregate prototype. 18 Convegno ANIDIS. Ascoli Piceno, Italy
- Senaldi IE, Guerrini G, Comini P et al (2020) Experimental seismic performance of a half-scale stone masonry building aggregate. *Bull Earthq Eng* 18:609–643. <https://doi.org/10.1007/s10518-019-00631-2>
- Sorrentino L, Alshawa O, Liberatore D (2014) Observations of out-of-plane rocking in the oratory of san Giuseppe dei Minimi during the 2009 L'Aquila earthquake. *Appl Mech Mater* 621:101–106. <https://doi.org/10.4028/www.scientific.net/AMM.621.101>
- Stavroulaki ME (2019) Dynamic behavior of aggregated buildings with different floor systems and their finite element modeling. *Front Built Environ*. <https://doi.org/10.3389/fbuil.2019.00138>
- Tomažević M, Weiss P, Velechovsky T (1991) The influence of rigidity of floors on the seismic behaviour of old stone-masonry buildings. *Eur Earthq Eng* 3:28–41
- Tomić I, Beyer K, Penna A et al (2019) Blind Prediction competition - SERA AIMS (Adjacent Interacting Masonry Structures). <https://doi.org/10.5281/zenodo.3607566>. Zenodo
- Tomić I, Penna A, DeJong M et al (2022a) Shake-table testing of a stone masonry building aggregate: Overview of blind prediction study. *Bull Earthq Eng Submitted*
- Tomić I, Penna A, DeJong M (2022b) Shake table testing of a half-scale stone masonry building. *Bull Earthq Eng Submitted*
- Valluzzi MR, Cardani G, Saisi A et al (2005) Study of the seismic vulnerability of complex masonry buildings. *Adv Archit Ser* 20:301–310

Vanin F, Penna A, Beyer K (2020) Equivalent-frame modeling of two shaking table tests of masonry buildings accounting for their out-of-plane response. *Front Built Environ*. <https://doi.org/10.3389/fbuil.2020.00042>

Publisher's Note Springer Nature remains neutral with regard to jurisdictional claims in published maps and institutional affiliations.